Environmental Science
Water Research & Technology

Rice Husk Based Nanocellulose Scaffold for Highly Efficient Removal of Heavy Metal Ions from Contaminated Water

Journal:	*Environmental Science: Water Research & Technology*
Manuscript ID	EW-ART-06-2020-000545.R1
Article Type:	Paper

Recent studies on drinking water quality have revealed that many parts of the world have been severely affected due to contamination caused by heavy metal ions. Even though many adsorptions/ absorption-based technologies have been examined for the removal of these toxic metal ions from contaminated water but are inexpensive and sustainable methods are still in necessity. Experimental results suggested that rice husk derived nanocellulose based adsorbent provide a suitable and environmentally viable solution for removal of (Pb(II) and La(III) toxic metal ions from water.

Rice Husk Based Nanocellulose Scaffold for Highly Efficient Removal of Heavy Metal Ions from Contaminated Water

Chengbo Zhan[a,b], Priyanka R. Sharma[b], Hongrui He[b], Sunil K. Sharma[b], Alexis McCauley-Pearl[c], Ruifu Wang[b], Benjamin S. Hsiao[b]*

[a] Space Institute of Southern China, Shenzhen 518117, China

[b] Department of Chemistry, Stony Brook University, Stony Brook, NY11794-3400, United States

[c] Smithtown High School East, Saint James, NY 11780, United States

C. Zhan: chengbo.zhan@gmail.com

P. R. Sharma: priyanka.r.sharma@stonybrook.edu

H. He: hongrui.he@stonybrook.edu

S. K. Sharma: sunil.k.sharma@stonybrook.edu

A. McCauley-Pearl: almp1101@gmail.com

R. Wang: ruifu.wang@stonybrook.edu

* B. S. Hsiao (Corresponding author): benjamin.hsiao@stonybrook.edu; Tel: +1(631)632-7793

Abstract

Rice husk is an agricultural residue of great annual production and has a high cellulose content. In this study, we have prepared highly charged carboxylcellulose nanofiber (CNF) from rice husk using the TEMPO-oxidation method and the extracted CNF was evaluated as an adsorbent for removal of lead(II) and lanthanum(III) (Pb(II) and La(III)) ions from contaminated water. Three different forms of nanocellulose adsorbent were prepared: suspension, freeze-dried, and nanocomposite containing magnetic nanoparticles, where their adsorption performance was tested against the removal of the two chosen heavy metal ions. The maximum adsorption capacity of rice husk based CNF was found to be the highest in nanocellulose suspension, i.e., 193.2 mg/g for Pb(II) and 100.7 mg/g for La(III). The separation of the used adsorbent in suspension was further facilitated by the gelation of CNF and metal cations, where the resulting floc could be removed by gravity-driven filtration. The absorption mechanism of the investigated CNF system is mainly due to electrostatic interactions between negatively charged carboxylate groups and multivalent metal ions. It was found that 90% of lanthanum content in the form of lanthanum oxychloride (determined by X-ray powder diffraction) could be obtained by incinerating the CNF/$LaCl_3$ gel. This study demonstrates a viable and sustainable solution to upcycle agricultural residue into remediation nanomaterials for removal and recovery of toxic heavy metal ions from contaminated water.

Keywords: nanocellulose; rice husk; adsorbent; heavy metal ions removal; water purification

1. Introduction

Exploiting underutilized material sources to extract effective sorptive materials is a sustainable and cost-effective way to tackle pressing global water challenges.[1, 2] As the food demand increases, the generation of agricultural residues during food production also increases. However, the conventional paths to process these "waste" materials often become not economically sustainable.[3] In this study, we demonstrate that the agricultural residues are an ideal and sustainable source to produce effective water purification sorptive materials, thus improving the nexus of food, energy and water systems.

Rice is a major food staple around the globe, where its annual production in 2017 was about 769 million tons worldwide according to the Food and Agriculture Organization in the UN. Rice husk is an inedible byproduct during the milling process to produce edible rice (brown or white). The tremendous amount of rice husk, which contains a mixture of cellulose, hemicellulose, lignin, and silica, has often been considered as an industrial raw material.[4] Rice husk could be a good material to produce activated carbon, and this process is often coupled with the process of silica extraction.[5, 6] Unlike the forestry (wood-based) products, rice husk has a high silica content (up to 20%) because silica is an essential component for the development and yield of rice.[7, 8] Silica is typically deposited over the stem, leaves and seeds of the rice plants, and provides the critical function of increasing the stem strength and sealing the epidermis to minimize water evaporation.[9, 10] However, the high inorganic content also hinders the biodegradation process of rice husk. To date, the most common treatment to deal with rice husk is by burning, where a great deal of progress has been made on converting rice husk into energy

output, such as fuel and electricity. The burnt ash can be used to produce silicon-based materials.[11, 12] However, the burning processes produce a very high volume of CO_2 emission, [13, 14] while the major part of the organic component in rice husk is completely wasted.

In addition to the efforts of extracting the silica from rice husk, extracting organics from rice husk is also economically attractive since rice husk is rich is proteins and oils.[15] There have been studies using nonpolar solvents, polar solvents, or enzyme-assisted aqueous solvents to extract rice bran oil.[16, 17] On the other hand, cellulose is a major component of rice husk. There have been several reports about the extraction of nanocellulose from rice husk, but none demonstrated the use of extracted nanocellulose as a water purification material.[18-20] In recent years, nanocellulose has been recognized as a sustainable nanomaterial with great potential in water purification, as it can be used as adsorbent, flocculant, coagulant, membrane material, or catalyst.[21-32] We believe that nanocellulose extracted from rice husk can also be used for this purpose to tackle the toxic metal contamination problems. In this study, lead(II) (Pb(II) or Pb^{2+}) and lanthanum(III) (La(III) or La^{3+}) were chosen as model contaminants. Lead is notorious for its high toxicity that can cause irreversible damage on neural systems and kidney, [33] as lead ions are not biodegradable and can be accumulated in the body through food or water consumption.[34] The second contaminant lanthanum is a rare earth element (REE), which has been widely used in electronic industry. In recent years, elevated environmental REE concentration has been detected in many regions.[35, 36] Besides the process of removing REE from water, recycling REE has also become desirable because of their low abundancy and high value. The adsorption for La(III) by varying adsorbents could be due to the interactions with hydroxyl, carboxyl, amino, or phosphoryl groups.[37-41] As a result, there have been several reports, utilizing biosorbents based

on algae, fish scale, and fruit peels in the raw state or with minimal chemical modifications to recycle lanthanum.[42-44]

In this study, we have prepared rice husk nanocellulose, which possesses abundant negatively charged carboxylate groups and extremely large specific surface area. This material should have good performance to adsorb positively charged metal ions, such as Pb(II)) and La(III).[45] The adsorption efficiency and corresponding mechanism of nanocellulose in three different forms: suspension, freeze-dried, and nanocomposite containing magnetic nanoparticles, were investigated and compared. The objective of this study was to develop a sustainable method to extract cellulose nanomaterials from rice husk for water purification. This approach can be complementary with other extraction methods to obtain useful components from rice husk, such as oils, proteins, and silica.

2. Experimental

2.1. Materials

Raw rice husk was obtained from Mexico. Sodium chlorite ($NaClO_2$), 2,2,6,6-tetramethyl-1- piperidinyloxy (TEMPO), sodium hypochlorite solution (NaClO, chlorine content: 10 – 15%), sodium bromide (NaBr) and sodium hydroxide (NaOH) were purchased from Sigma-Aldrich; lead nitrate ($Pb(NO_3)_2$ was purchased from Acros; ferric chloride hexahydrate

($FeCl_3$•$6H_2O$), ferrous chloride hydrate ($FeCl_2$•xH_2O), lanthanum chloride ($LaCl_3$), lead acetate ($Pb(OAc)_2$) and lead nitrate ($Pb(NO_3)_2$) were purchased from Fisher Scientific. All chemicals were used without further purification.

2.2. Materials Preparation

2.2.1. Preparation of Rice Husk Carboxylcellulose Nanofibers (RHCNF)

Raw rice husk of length (≤5 mm) was delignified at 80 °C for 2 h using sodium hydroxide solution (1 mol/L) with a 10:1 solvent to biomass ratio. After the base treatment, delignified rice husk was washed with deionized (DI) water and dried in oven. The dried sample was then bleached 2 times using an acidic solution of sodium chlorite (1% w/v, the pH was decreased around 4 by glacial acetic acid) with a 30:1 solvent to biomass ratio at 70 °C for 1 h. The product was then rinsed by DI water, dried and stored. TEMPO-mediated oxidation was carried out on the treated (bleached) rice husk sample using a previously reported procedure.[46] In brief, bleached rice husk (10 g, 61.7 mmol) was suspended in DI water (960 mL), to which NaBr (1 g, 9.72 mmol) and TEMPO (0.1 g, 0.64 mmol) were added. The suspension was kept stirring for 15 min until TEMPO and NaBr were fully dissolved, and NaClO (75 g, 12% aqueous solution, 121 mmol) was subsequently added to the mixture. During the reaction, the pH value of the suspension was maintained between 10 and 10.5 by using a NaOH solution (0.1 mol/L). After 24 h, the reaction was terminated with addition of 10 mL ethanol. The oxidized fibers slurry was dialyzed against DI water until the conductivity of the dialysate was below 5 μS (after

equilibration for 12 h). Finally, the slurry was mechanically defibrillated with a homogenizer (GEA Niro Soavi, Panda Plus) operated at 200 bars for 3 cycles. One part of the suspension was freeze-dried for characterization (solid state NMR, SEM, TGA, and XRD). The rest of the suspension was diluted into varying concentrations for the adsorption test.

2.2.2. Synthesis of Magnetic Nanoparticles

To prepare magnetic nanoparticles, $FeCl_3 \cdot 6H_2O$ (0.1 g, 0.37 mmol) and $FeCl_2 \cdot 4H_2O$ (0.0397 g, 0.20 mmol) were first dissolved in 50 mL of water. 50 mL of NaOH solution (0.1 M) was subsequently added to the solution, where the temperature was raised to 80 ^oC. The mixture was kept stirring for 3 h to form magnetic nanoparticles. After the reaction, the resulting black precipitants were separated by centrifugation and washed twice by DI water.[47]

2.2.3. Synthesis of Magnetic Nanocellulose Composite (Mag-RHCNF)

The magnetic nanoparticles prepared above was resuspended in 50 mL of DI water, where 100 mL of rice husk-based CNF suspension (0.465 wt%) was subsequently added. The mixture was heated to 80 ^oC and the reaction was stopped after 2 h. The product was washed by DI water and centrifuged 3 times and freeze-dried.

2.3. Characterization

2.3.1. Zeta Potential Measurements

Zeta potential of the RHCNF sample was measured by a Zetaprobe Analyzer (Colloid Dynamics) equipped with the pH electrode and ESA sensor probe. Before analyzing the sample, the pH electrode was calibrated using 3 different pH buffer standards (pH = 4.01, 7.01 and 10.01). The ESA sensor was calibrated using the standard zeta probe polar solution (KSiW solution). Upon the completion of calibration test, the RHCNF suspension (0.2 wt%, 280 mL) was added to the sample holder, where the pH probe and the ESA sensor was then inserted. During the measurement the sample was under continuous stirring by a mixer.

2.3.2. Fourier Transform Infra-Red Spectrometry (FTIR)

A Nicolet iS20 FTIR Spectrometer (Thermo Fisher Scientific) was used to measure the IR spectra in the transmission mode, where the spectra were taken between 400 and 4000 cm^{-1}. A total of 16 scans were taken per sample. The RHCNF sample was recorded in the attenuated total reflectance (ATR) mode with a resolution of 0.5 cm^{-1}.

2.3.3. ^{13}C CPMAS NMR

Solid state ^{13}C CPMAS NMR measurements of RHCNF were carried out by a Bruker Utrashield 500WB plus (500 MHz) instrument, equipped with a 2.5 mm triple resonance magic angle spinning (MAS) probe. The resonance frequency for ^{13}C was 10,000 Hz and the samples were spun at the magic angle with a speed of 12 KHz.

2.3.4. X-Ray Diffraction (XRD)

XRD measurements of RHCNF and incinerated gel were carried out using a Benchtop Rigaku MiniFlex 600 instrument. The samples were loaded on a zero-diffraction silicon plate. The Cu Kα radiation was generated at 40 kV and 40 mA (λ = 0.154 nm) using a Ni filter. Data collection was carried out using a flat holder in the Bragg-Brentano geometry (5-70°).

2.3.5. Thermogravimetric Analysis (TGA)

TGA was performed by a Q50 thermogravimetric analyzer (TA Instruments). About 10 mg of RHCNF samples was loaded on the platinum pan and then heated up from 25 ^{o}C to 800 ^{o}C at a heating rate of 10 ^{o}C/ min under dry nitrogen flow. The weight loss (%) of samples were recorded as a function of temperature.

2.3.6. Transmission Electron Microscopy (TEM)

TEM images of RHCNF and varying floc samples were acquired by a JEM-1400 microscope (JEOL). In the typical TEM measurement, 2 μL of RHCNF suspension at the 0.01 wt% concentration was deposited on a glow-discharged 300 mesh copper grid with carbon film coating. The operating voltage for the TEM measurement was 120 kV. The TEM image analysis was performed by ImageJ software.

2.3.7. Scanning Electron Microscopy (SEM)

SEM test was performed by a Crossbeam 340 scanning electron microscope (Carl Zeiss Microscopy) equipped with the capability of energy dispersive spectroscopy (EDS, X-Max 50, Oxford Instruments). Freeze-dried RHCNF samples before and after the adsorption test were loaded on the sample holder by a piece of carbon tape for acquisition of SEM images. The measurements were carried out with a SE detector at 3kV of electron high tension (EHT) and elemental mappings were collected at 20kV of EHT.

2.3.8. Atomic Forced Microscopy (AFM)

AFM measurement was performed in the tapping mode using a Bruker Dimension ICON scanning probe microscope (Bruker Corporation, U.S.A.) equipped with a Bruker OTESPA tip (radius 7 nm). A Piranha cleaned silica wafer substrate was immersed in RHCNF suspension (0.0015 wt%) for overnight and taken out before measurement. NanoScope Analysis, a software by Bruker, was used for all the AFM image analysis.

2.4. Static Adsorption Test

Lanthanum chloride, lead acetate and lead nitrate stock solutions were prepared at concentrations ranging from 10 to 2000 ppm. For the adsorption capability study of RHCNF and

Mag-RHCNF, about 5 mg of the solid sample was added to 2 mL of the metal ion solution. To test the adsorption capacity of the RHCNF suspension, 2 mL of metal ion solution was mixed with 2 mL of 0.12 wt% RHCNF suspension. After adsorption of metal ions, the mixture from the above adsorbent (freeze-dried RHCNF, Mag-RHCNF and RHCNF suspension) was centrifuged, where the supernatant was collected. The supernatant was diluted down to the level of 100 ppb, and the exact ion concentration was analyzed using the inductively coupled plasma mass spectrometry (ICPMS) technique (SQ-ICP-MS, Thermo Fisher Scientific). Based on the adsorption rates at various concentrations, and at different pH values, an isotherm curve was generated. The maximum adsorption capacity for the metal ions was determined by the Langmuir model as follows:

$$q = \frac{Kq_m c}{1 + Kc}$$

where q is the adsorption capacity with concentration of adsorbate at c when equilibrium is reached, q_m is the maximum capacity of the adsorbent, and K is the Langmuir constant.

3. Results and Discussion

3.1. Characterization of RHCNF and RHCNF-Based Adsorbents

RHCNF was prepared from TEMPO-mediated oxidation of rice husk after delignification/bleaching treatments. The introduction of carboxyl groups on RHCNF was

confirmed by FT-IR and ^{13}C solid-state NMR measurements and their results are shown in Figure 1. It was seen that the peak at 1600 cm^{-1} in the IR spectrum (Figures 1A) and the peak at 171 ppm in the NMR spectrum (Figure 1B) could be assigned to the carboxyl groups, confirming that the process of TEMPO-mediated oxidation was successfully carried out to fabricate RHCNF. It was also found that the peaks assigned to lignin syringyl (153 ppm in the NMR spectrum) and lignin guaiacyl units (171 ppm in the NMR spectrum) disappeared in RHCNF, indicating that the lignin components were completely removed.[48, 49] The carboxyl content of RHCNF was further determined by the conductometric titration as 1.10 mmol/g, and the zeta-potential was about -55 mV. These results indicated that RHCNF possessed a negatively charged surface. Subsequently, the morphology of RHCNF was determined by TEM and AFM methods (results shown in Figures 1C and 1D). It was found that RHCNF exhibited the fibrous morphology with average width about 5 nm and length at micrometer scale, confirming that RHCNF possessed a high aspect ratio and very high specific area. The RHCNF sample was also characterized by the XRD technique (Figure 1E), where results exhibited typical diffraction peaks of cellulose crystals. Compared with the XRD profiles between raw rice husk and RHCNF, the results indicated that the amorphous part of raw rice husk had been largely removed. The above results suggested that RHCNF possessed high crystallinity, a large amount of carboxyl groups, and high surface area with great potential as an effective adsorption agent to remove cationic contaminants.

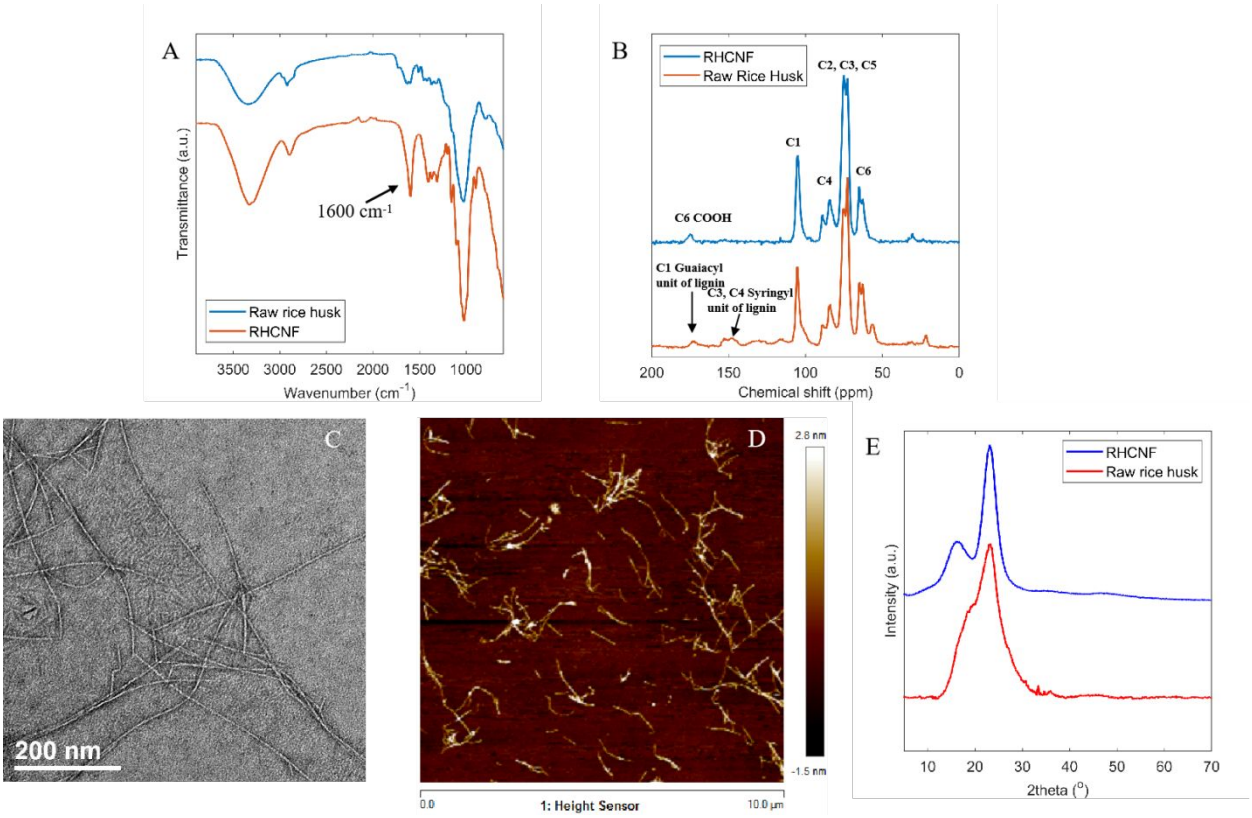

Figure 1. Characterizations of RHCNF with (A) FT-IR, (B) solid state ^{13}C CPMAS NMR, (C) TEM, (D) AFM and (E) XRD techniques. The comparison of raw rice husk and RHCNF ((A), (B) and (E)) confirmed the successful preparation of TEMPO-mediated oxidized cellulose nanofibers. The microscopic results ((D) and (E)) confirmed the fiber morphology of RHCNF.

In this study, RHCNF-based adsorbents in three different formats were evaluated: RHCNF suspension, freeze-dried RHCNF and RHCNF-based nanocomposite containing magnetic nanoparticles (Meg-RHCNF). The RHCNF suspension was in the original state of nanocellulose product after TEMPO oxidation and defibrillation treatments, so it required no additional processing. It was found that the RHCNF suspension could form gel after adsorption of multivalent metal ions, such that the used adsorbent could be easily removed from the treated water. The separation of the gelled RHCNF-metal ions floc from water was demonstrated in the

Supporting Information, where the gel could be filtered out from water using a commercial coffee filter having a mesh size about 100 μm (Figure S1) by gravity.

The solid RHCNF adsorbent could be produced by freeze-drying the RHCNF suspension. As the freeze-drying process can remove more than 99.5 wt% of water from the RHCNF suspension, the total weight and volume of RHCNF adsorbent would become considerably reduced, thus saving a great deal of transportation cost. However, as dried RHCNF cannot be easily dispersed in water, the removal of consumed RHCNF requires the use of ultrafiltration with smaller membrane size, or application of centrifugation to separate the secondary contaminant from treated water, thus imposing higher energy consumption than the removal of gel floc,

To overcome this problem, we also prepared a magnetic composite scaffold (Mag-RHCNF), consisting of iron oxide nanoparticles anchored in the RHCNF scaffold, as a solid adsorbent. The adoption of Mag-RHCNF would enable us to use magnetic separation to separate the secondary contaminant from water, which has been demonstrated in some water treatments.[50, 51] The characterization of Mag-RHCNF is described in the Supporting Information. The successful incorporation of nanoscale magnetic nanoparticles (Figure S2, the average diameter of the nanoparticles was about 2.8 nm) in the RHCNF scaffold was confirmed by SEM (Figure S3), TGA (Figure S4A) and XRD (Figure S4B) experiments. The chosen content of magnetic nanoparticles loaded in Mag-RHCNF composites was about 7 wt%. Based on the XRD profile, the observed diffraction peaks from the nanoparticles indicated that they consisted of the spinel

phase of Fe_3O_4 crystals.[52] This iron oxide phase has been shown to be a ferrite with properties of the magnetite.[53] A demonstration of magnetic-assisted separation using Mag-RHCNF could be seen in Figure S5. The adsorption efficiency of these three adsorbents for two model metal ions (i.e., La(III) and Pb(II)) are as follows.

3.2. Adsorption Performance Against $LaCl_3$

$LaCl_3$ was chosen as a representative heavy metal ion compound form the rare earth element group. Two adsorption studies: adsorption kinetics and adsorption capacity, of all three RHCNF adsorbents in different format against La(III) were conducted. The adsorption kinetics evaluation from the solid RHCNF and Mag-RHCNF adsorbents was carried out by using 250 ppm of metal ions, where the results are shown in Figure S5. It was seen that the maximum adsorption capacity was achieved around 24 h, which was used as the time period for all the static adsorption study. The static adsorption evaluation of the maximum adsorption capacity was carried out by adding 2 mL of RHCNF suspension or 5 mg of solid adsorbent (RHCNF and Mag-RHCNF) into 2 mL of a La(III) solution at varying concentration (i.e., 10, 25, 50, 100, 250, 500, 1000 ppm). After 24 h of adsorption, the concentration of La(III) was measured to calculate the equilibrium concentration of adsorbate (C_e) and the amount of adsorbate adsorbed at equilibrium concentration (q_e). The adsorption isotherms of RHCNF suspension, freeze-dried RHCNF and Mag-RHCNF adsorbents for $LaCl_3$ removal at pH = 7 are depicted in Figure 2A. These isotherms were fitted by the nonlinear Langmuir equation to estimate the maximum adsorption capacity (q_m). It was found that the q_m value was 100.7 mg/g for the RHCNF

suspension, 59.0 mg/g for freeze-dried RHCNF and 41.4 mg/g for Mag-RHCNF. This trend could be correlated with the carboxylate content of the adsorbent. The carboxylate content of the adsorbent was determined by the conductometric titration method, where the results indicated that it was 1.10 mmol/g for the RHCNF suspension, 0.73 mmol/g for freeze-dried RHCNF, and 0.46 mmol/g for Mag-RHCNF. The above observations suggested that the adsorption capacity of the adsorbent against La(III) was highly dependent on the carboxylate content. The RHCNF suspension, with the highest carboxylate content, exhibited the best adsorption performance. The freeze-dried RHCNF showed the second-best adsorption performance. This is reasonable because the freeze-dried RHCNF sample could not be fully defibrillated in water, leading to some hidden surface area not available for adsorption (ionic interaction). The lowest carboxylate content on Mag-RHCNF suggested that some carboxylate functional groups (negatively charged) were probably consumed by the anchoring of metal oxide nanoparticles (positively charged). The adsorption capacity and efficiency of the RHCNF suspension against La^{3+} ions at pH = 7 with the concentration range of 10 – 1000 ppm are shown in Table 1. It was found that the adsorption efficiency increased with the decrease in La(III) concentration. This behavior is quite desirable for recovery of La^{3+} ions from highly diluted sources.

Table 1. Adsorption capacity and efficiency of the RHCNF suspension against La^{3+} ions at pH = 7 in the concentration range of 10 – 1000 ppm, at pH 7 and room temperature.

Original La^{3+} conc. (ppm)	Final La^{3+} conc. (ppm)	RHCNF content[a] (0.12 wt%)/2 mL (mg)	Experimental adsorption capacity (q_e, mg/g)	Adsorption efficiency[b]
1000	898	2.4	85.0 ± 6.50	0.102
500	412	2.4	73.3 ± 1.51	0.176
250	192	2.4	48.8 ± 5.93	0.232
100	68.9	2.4	25.9 ± 5.40	0.311
50	25.6	2.4	20.4 ± 7.04	0.488
25	5.38	2.4	16.4 ± 8.41	0.785
10	1.23	2.4	7.31 ± 3.47	0.877

[a] Total amount of RHCNF used in 2 mL of 0.12 wt% suspension was 2 g × 0.12%= 2.4 mg.
[b] Adsorption efficiency = (Original conc. – Final conc.) / Original conc.

The pH effect on the adsorption performance of the RHCNF suspension was also studied to reveal the adsorption mechanism. The results are illustrated in Figure 2B. It was seen that the adsorption capacity increased under the basic conditions, which was probably due to the precipitation of lanthanum hydroxides. In contrast, the adsorption capacity was considerably reduced under the acidic conditions. The reason for this behavior was probably due to the protonation of carboxylate groups at low pH values. To test this hypothesis, the zeta-potential of the RHCNF suspension under those low pH conditions was measured, and the results are shown in Figure 2B. It was found that at low pH values, the zeta-potential of the RHCNF suspension was significantly elevated, which indicated that the negative charge density on the RHCNF surface was greatly reduced.[54] The decrease in negative charges would result in weaker interactions between the adsorbent and La^{3+} ions, thereby leading to the decrease in adsorption capacity. The results indicated that the RHCNF in suspension possessed high efficiency at neutral or high pH values, but the performance would be reduced at low pH values.

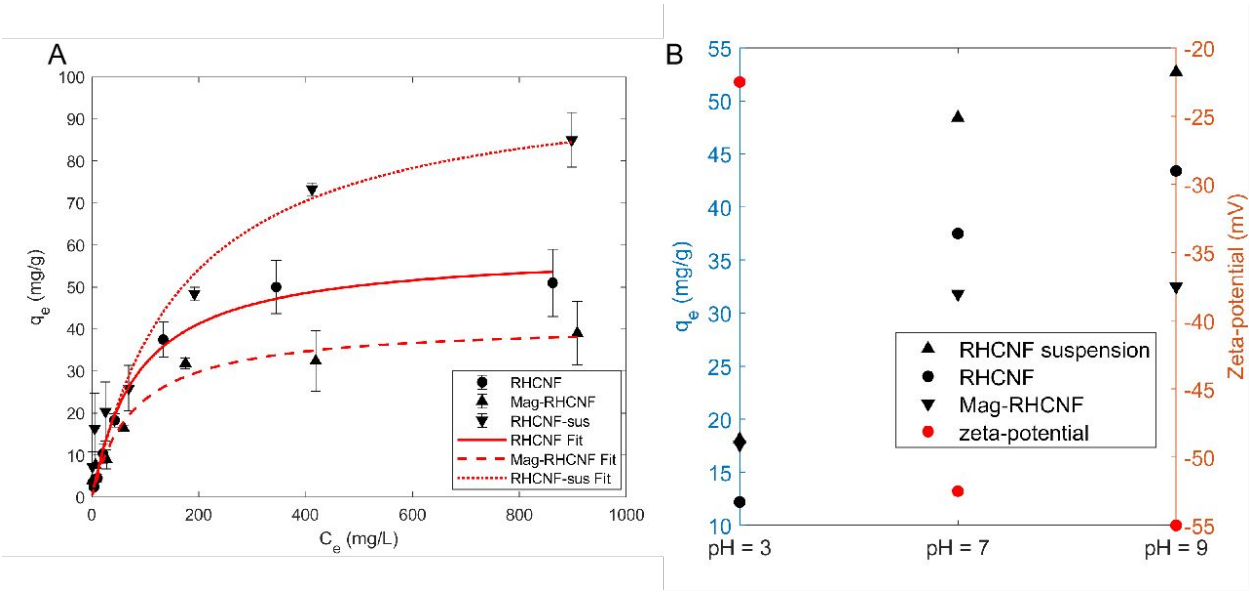

Figure 2. (A) The adsorption isotherms of RHCNF suspension, freeze-dried RHCNF and Mag-RHCNF adsorbents for La(III) (i.e. $LaCl_3$) removal. The initial La(III) concentration was 10, 25, 50, 100, 250, 500, 1000 ppm; (B) the adsorption capacity of different adsorbent at different pH values (pH = 3, 7, 9) with an initial La(III) concentration of 250 ppm, and the corresponding zeta-potential of RHCNF samples in suspension. All the measurements above mentioned were conducted at pH = 7 and room temperature. The dosage of adsorbent was 5 mg for solid samples (freeze-dried RHCNF and Mag-RHCNF) and 2 mL for 0.12 wt% RHCNF suspension.

3.3. Adsorption Performance Against $Pb(OAc)_2$

$Pb(OAc)_2$ was chosen as a second representative contaminant for toxic heavy metal ions, and research has demonstrated the capability of carboxylcellulose nanofibers to adsorb Pb(II).[55] The kinetics and static adsorption studies were carried out using the same procedures as in the above La(III) studies. The adsorption isotherm results of RHCNF suspension, freeze-dried RHCNF and Mag-RHCNF absorbents for Pb(II) (i.e., $Pb(OAc)_2$) removal are shown in Figure 3A. These isotherms were also analyzed by the nonlinear Langmuir equation, yielding the q_m

value of 193.2 mg/g for RHCNF suspension, 170.4 mg/g for freeze-dried RHCNF and 52.9 mg/g for Mag-RHCNF. The adsorption capacity of the different adsorbent at different pH values using an initial La(III) concentration of 250 ppm is shown in Figure 3B. Unlike the case of $LaCl_3$, the adsorption capacity for RHCNF suspension for $Pb(OAc)_2$ removal only showed a slight decrease at the low pH value. The latter behavior could not be correlated with the zeta-potential values of RHCNF suspensions at different pH values, indicating that the adsorption of $Pb(OAc)_2$ by RHCNF in suspension was not totally dependent on the surface charge of RHCNF.

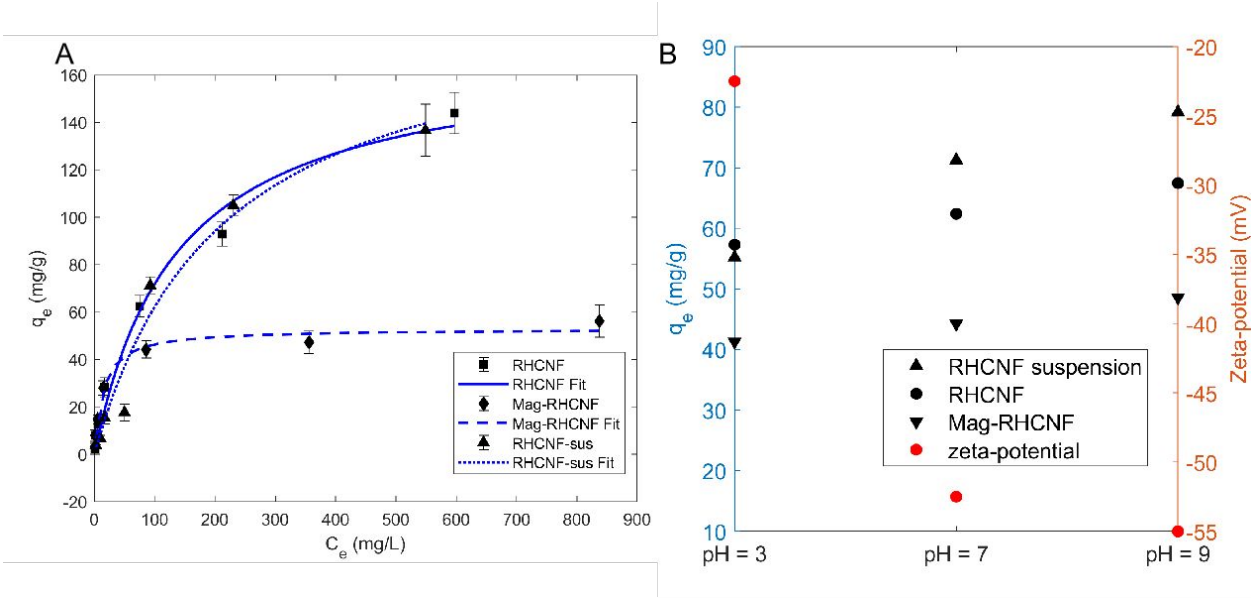

Figure 3. (A) The adsorption isotherms of RHCNF suspension, freeze-dried RHCNF and Mag-RHCNF adsorbents for Pb(II) (i.e. $Pb(OAc)_2$) removal. The initial Pb (II) concentration was 10, 25, 50, 100, 250, 500, 1000 ppm; (B) the adsorption capacity of different adsorbent at different pH values (pH = 3, 7, 9) with an initial Pb(II) concentration of 250 ppm and the zeta-potential of RHCNF suspension. All the measurements above mentioned were conducted at pH = 7 and room temperature. The dosage of the adsorbent was 5 mg for solid samples (freeze-dried RHCNF and Mag-RHCNF) and 2 mL for 0.12 wt% RHCNF suspension.

We hypothesize that the different adsorption behavior of using RHCNF to remove $Pb(OAc)_2$ followed the dissociation property of the compound rather than the electrostatic

interactions between RHCNF and Pb^{2+} ions. To verify this hypothesis, the adsorption study of RHCNF was further carried out using $Pb(NO_3)_2$, which is an ionic salt that can fully dissociate in water. The comparison of the different adsorption isotherms of using the RHCNF suspension to remove $Pb(OAc)_2$ versus $Pb(NO_3)_2$ from water is illustrated in Figure 4A. Based on this diagram, the RHCNF suspension exhibited the maximum adsorption capacity for $Pb(NO_3)_2$ of 150.0 mg/g, which was not as high as that for $Pb(OAc)_2$ (193.2 mg/g). However, the pH test results were also different. Figure 4B showed that $Pb(NO_3)_2$ exhibited a notable decrease in the adsorption capacity at low pH values, which was similar to the case of $LaCl_3$. Thus, we verified the hypothesis that the adsorption behavior against $Pb(OAc)_2$ was more related to its dissociation state rather than the electrostatic interactions between metal ions and RHCNF.

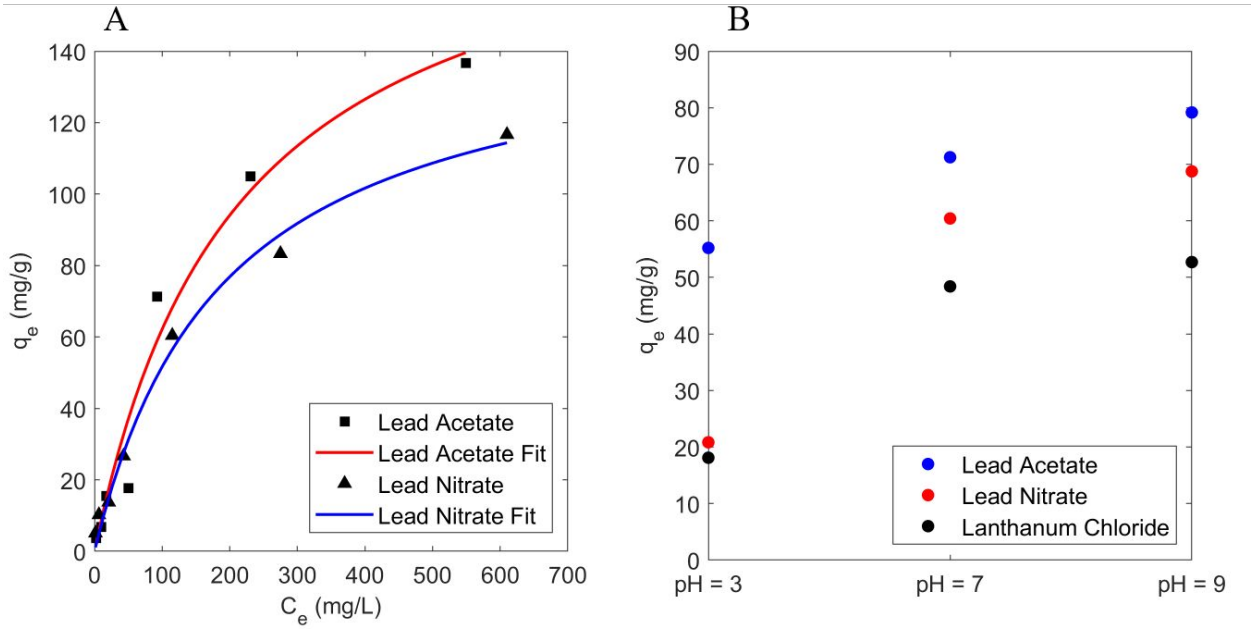

Figure 4. (A) The adsorption isotherms of RHCNF suspension for $Pb(OAc)_2$ and $Pb(NO_3)_2$ removal. The initial Pb (II) concentration was 10, 25, 50, 100, 250, 500, 1000 ppm; (B) the adsorption capacity of RHCNF suspension for $LaCl_3$, $Pb(OAc)_2$ and $Pb(NO_3)_2$ with the initial metal concentration of 250 ppm. All the measurements were conducted at pH = 7 and room temperature. The dosage of the adsorbent was 2 mL for 0.12 wt% RHCNF suspension.

3.4. The Adsorption Mechanism of RHCNF Adsorbent

The adsorption study for $LaCl_3$ showed that the adsorption capacity of RHCNF was closely related to the carboxylate content of the adsorbent, where the capacity significantly decreased at low pH values. However, the adsorption capacity for $Pb(OAc)_2$ of RHCNF was not sensitive to the pH change. The difference in the adsorption behavior indicated that the removal of these two contaminants exhibited different mechanisms, which were revealed by TEM and XRD measurements.

The XRD and TEM results from characterizations of the gel floc samples formed by mixing RHCNF suspension and varying metal ion solutions are shown in Figure 5. In Figure 5A, the XRD pattern of RHCNF-La(III) gel was almost identical to that of pristine RHCNF, which suggested that no notable occurrence of mineralization after La(III) adsorption. The TEM results (Figure 5B) also showed clear fibrous morphology of RHCNF after adsorption with no signs of inorganic entity, even though the fiber width was found to increase to about 10 nm due to interfibrillar aggregation. This suggests that the La^{3+} ions behaved like ionic cross-linking agents, binding the adjacent RHCNF and form fiber aggregates. In contrast, the XRD pattern of RHCNF-$Pb(OAc)_2$ gel floc exhibited sharp diffraction peaks, indicating the presence of lead hydroxide ($Pb(OH)_2$) crystals formed by mineralization. The presence of lead hydroxide crystals was also evident in the TEM image (Figure 5C), where elongated crystalline regions extruded from the RHCNF were seen. The higher maximum adsorption capacity of RHCNF suspension

for $Pb(OAc)_2$ that for $Pb(NO_3)_2$ could thus be understood, as the former was dominated by the mineralization of lead hydroxide crystals.

The difference in adsorption mechanism could also account for the adsorption results from mixed solutions (Table S1, Supporting Information), indicating the competition of different metal ions during the adsorption process. The results showed that the adsorption capacity of $Pb(OAc)_2$ continuously increased with time but the adsorption of $LaCl_3$ remained about constant (after saturation). This indicated that the charged-induced adsorption of La(III) was limited by the available adsorption sites (carboxylate groups) in RHCNF, but the limiting factors in the adsorption of Pb(II) included not only the adsorption sites but also the mineralization process of $Pb(OH)_2$ crystal formation.

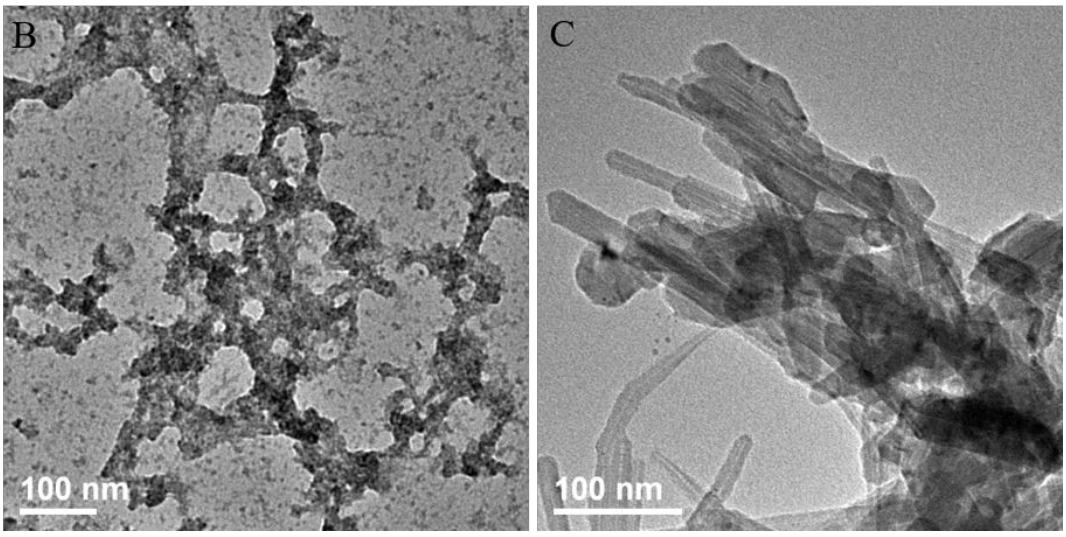

Figure 5. Characterization of the gel floc formed by mixing RHCNF suspension with metal ion solutions. (A) The XRD patterns of pristine RHCNF, RHCNF-$LaCl_3$ gel, and RHCNF-$Pb(OAc)_2$ gel, where the diffraction peak from (110) plane of lead hydroxide could be clearly observed (peaks marked by # belong to lead hydroxide). The spectra were vertically shifted for better clarity. (B) TEM image of RHCNF-$LaCl_3$ gel. (C) TEM image of RHCNF-$Pb(OAc)_2$ gel.

The different adsorption behavior between removal of $LaCl_3$ versus $Pb(OAc)_2$ could also be explained as follows. $LaCl_3$ is an ionic salt that fully dissociates in aqueous solution, where La^{3+} ions can interact with the $-COO^-$ groups, but much weaker with the neutral -COOH groups. Therefore, the adsorption capacity was significantly reduced when the carboxylate groups were

protonated at the low pH value. As for $Pb(OAc)_2$, the dissociation constant is 9.4×10^{-9} mol/L and the major ionic species is $Pb(OAc)^+$.[56] Taking a 100 ppm solution for consideration, which is an median concentration solution, the lead acetate concentration was about 3.0×10^{-4} mol/L. Thus, the concentration of dissociated species was only about 1.7×10^{-6} mol/L, indicating that only less than 1% of $Pb(OAc)_2$ was dissociated. Thus, the adsorption for $Pb(OAc)_2$ was not sensitive to the low pH conditions. Therefore, we concluded that for dissociated metal ions, the adsorption took place on the surface of cellulose nanofibers and the driving force was the electrostatic interactions between negatively charged carboxylate groups and the cations.[57, 58] In contrast, for weakly dissociated salts, the combined effects of the RHCNF surface-induced mineralization and electrostatic interactions led to the removal of the contaminant.

3.5. Recovery of Lanthanum

A comparison of different adsorbents and their reported adsorption capacity values for La(III) removal is listed in Table 2. It was found that the RHCNF suspension exhibited the highest adsorption capacity among all adsorbents tested, including polymers and inorganic materials. However, the RHCNF suspension system may offer some additional advantages. One is that RHCNF suspension is more sustainable than synthetic polymeric adsorbents for water purification, as the RHCNF adsorbent system is extracted from rice husk that is extremely abundant and low-cost. Another advantage is that the RHCNF suspension can offer an easy pathway for lanthanum recovery because lanthanum is a rare metal ion and extensively used for various important applications which include electronics, medical and nuclear industry.[35]

However, the desorption process of lanthanum from inorganic adsorbents would require strong acid treatment. [59-61] In this section, we further demonstrated a simple lanthanum recovery method, which involved the thermolysis of the RHCNF-La suspension or gel. It has been shown that RHCNF suspension could form gel floc when it encountered La^{3+} ions. The resulting gel floc, containing nanocellulose and La(III) content, could be easily separated by low energy microfiltration (Figure S1). The most efficient way to recover the lanthanum compound is by incineration of the gel floc, where the organic scaffold can be reduced leaving behind mainly the inorganic element. In this demonstration, we collected the gel floc from the addition of 20 mL of 0.12 wt% RHCNF suspension and 20 mL of 2000 ppm $LaCl_3$ solution and then incinerated the mixture at 500 ^{o}C in air. The weight of the resulting residue (white powder) was 2.6 mg, where the corresponding XRD pattern is shown in Figure 6. In this pattern, the initial peaks from nanocellulose disappeared completely, where the newly emerging peaks perfectly matched the diffraction profile of lanthanum oxychloride (LaOCl)[62] with high purity. Based on the adsorption capacity of RHCNF suspension (85.0 mg/L in Table 1), the weight of the adsorbent (24 mg) and the product of lanthanum oxychloride (LaOCl), we calculated the theoretical yield to be 2.8 mg. Thus, the recovery ratio was found to be 92.3%. The results suggested that the RHCNF suspension could be used to effectively remove and recovery lanthanum from contaminated water.

Although the incineration process seems to be a method not environmentally friendly and is associated with high energy consumption, this treatment is still worth considering based on the life cycle analysis and practicality. For example, due to the limited space in landfill, one popular disposal approach for solid waste is incineration, where the heat coupled with this process can be

converted to electricity.[11] In addition, the high temperature combustion (could be up to 900 °C) process is routinely used to produce silica and activated carbon.[7] As compared to production of activated carbon, our demonstration of the RHCNF production and the post-incineration step for recovery of precious metal is comparable in the perspective of environmentally sustainability as the RHCNF decomposition takes place at lower temperatures (around 500 °C). We believe the demonstrated CNF adsorbent system could be a viable solution to recover rare-earth elements from industrial wastewater.

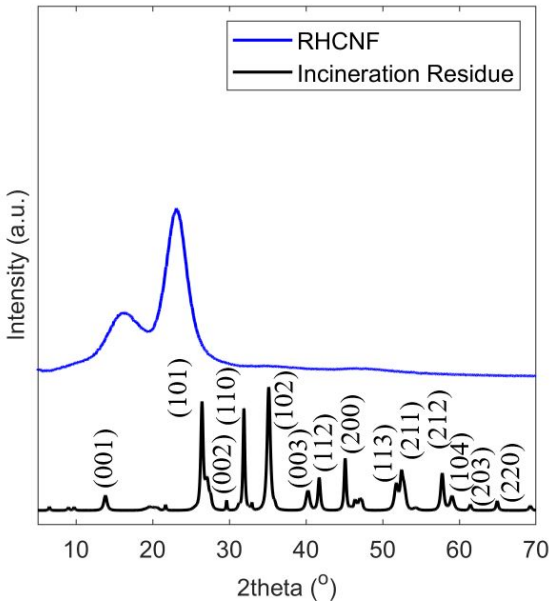

Figure 6. The XRD pattern of RHCNF and the incineration residue of the gel floc formed by mixing of RHCNF suspension and $LaCl_3$ solution. The peaks of the incineration residue could be assigned to lanthanum oxychloride (LaOCl), where the indices of diffraction peaks are shown.

Table 2. Comparison of the La(III) adsorption capacity for the RHCNF suspension with those from other adsorbents.

Adsorbent	Maximum adsorption capacity (mg/g)	ref
RHCNF suspension	100.3	This work
Algae	~100	42
Amine modified activated carbon	66.2	59
Clay	35.9	60
Zeolite and bentonite	0.45	61
Amino phosphate modified nanotitania	14.33	63
Magnetic alginate-chitosan gel	97.1	64
Polydopamine complex membranes	59.5	65
Durian rind pectin	41.2	66

4. Conclusions

In this study, TEMPO-oxidized rice husk cellulose nanofibers (RHCNF) were prepared into 3 different forms as adsorbents (suspension, freeze-dried, and nanocomposite containing magnetic nanoparticles). Three model contaminants, $LaCl_3$, $Pb(OAc)_2$ and $Pb(NO_3)_2$ were also used in the adsorption study. All 3 adsorbent systems exhibited good removal performance against the contaminants, while the RHCNF suspension exhibited the highest adsorption capacity and the resulting RHCNF-metal ion floc could be separated by gravity-driven microfiltration. However, the chosen contaminants exhibited different adsorption mechanisms: (i) for ionic salts: $LaCl_3$ and $Pb(NO_3)_2$, the adsorption was dominated by the electrostatic interactions between the carboxylate groups and multivalent metal ions; and (ii) for salt with weak dissociation: $Pb(OAc)_2$, the contaminants deposited on the adsorbent surface which could lead to the mineralization process. We further demonstrated that after incineration of the RHCNF/La(III) gel floc at 500 °C, the nanocellulose scaffold could be completely decomposed and over 92% of lanthanum could

be recovered in the form of LaOCl crystals with high purity. The results indicated that rice husk could be a sustainable source to extract value-added nanocellulose for water purification.

Conflicts of interest

No potential conflict of interest was declared by the authors.

Acknowledgement

The financial support for this work was provided by a grant from the Polymer Program of the Division of Materials Science in the National Science Foundation (DMR-1808690). This research used electron microscopy instruments in the Center for Functional Nanomaterials at Brookhaven National Laboratory, which is a U.S. DOE Office of Science Facility (Contract No. DE-SC0012704). The authors further thank Dr. Chung-Chueh Chang at the Advanced Energy Research and Technology Center in Stony Brook University for his assistance of the TGA measurement, and Ms. Katie Wooton at the Facility for Isotope Research and Student Training in Stony Brook University for her help with the ICP-MS study.

References

1. J. Diamond, *Collapse: How societies choose to fail or succeed*, Penguin, 2005.

2. P. R. Sharma, S. K. Sharma, T. Lindström and B. S. Hsiao, *Adv Sustainable Syst*, 2020, **4**, 2070009.
3. K. Foo and B. Hameed, *Adv Colloid Interf Sci*, 2009, **152**, 39-47.
4. T. N. Ang, G. C. Ngoh, A. S. M. Chua and M. G. Lee, *Biotechnol Biofuels*, 2012, **5**, 67.
5. M. M. Alam, M. A. Hossain, M. D. Hossain, M. Johir, J. Hossen, M. S. Rahman, J. L. Zhou, A. Hasan, A. K. Karmakar and M. B. Ahmed, *Processes*, 2020, **8**, 203.
6. M. Asadullah, M. S. Kabir, M. B. Ahmed, N. A. Razak, N. S. A. Rasid and A. Aezzira, *Korean Journal of Chemical Engineering*, 2013, **30**, 2228-2234.
7. N. Soltani, A. Bahrami, M. Pech-Canul and L. González, *Chem Eng J*, 2015, **264**, 899-935.
8. J. F. Ma, K. Tamai, N. Yamaji, N. Mitani, S. Konishi, M. Katsuhara, M. Ishiguro, Y. Murata and M. Yano, *Nature*, 2006, **440**, 688-691.
9. J. F. Ma, *Soil Sci Plant Nutr*, 2004, **50**, 11-18.
10. N. Mitani, J. F. Ma and T. Iwashita, *Plant Cell Physiol*, 2005, **46**, 279-283.
11. A. Faaij, *Mitig Adapt Strateg Glob Change*, 2006, **11**, 343-375.
12. J. C. Marchal, D. J. Krug III, P. McDonnell, K. Sun and R. M. Laine, *Green Chem*, 2015, **17**, 3931-3940.
13. J. Sun, H. Peng, J. Chen, X. Wang, M. Wei, W. Li, L. Yang, Q. Zhang, W. Wang and A. Mellouki, *J Clean Prod*, 2016, **112**, 2625-2631.
14. S. Pongpiachan, M. Hattayanone and J. Cao, *Atmos Pollut Res*, 2017, **8**, 1069-1080.
15. Y. P. Pal and A. P. Pratap, *J Oleo Sci*, 2017, **66**, 551-556.
16. N. Pengkumsri, C. Chaiyasut, B. S. Sivamaruthi, C. Saenjum, S. Sirilun, S. Peerajan, P. Suwannalert, S. Sirisattha, K. Chaiyasut and P. Kesika, *Food Sci Technol*, 2015, **35**, 493-501.
17. P. Hanmoungjai, D. Pyle and K. Niranjan, *JAOCS*, 2001, **78**, 817-821.
18. N. Johar, I. Ahmad and A. Dufresne, *Ind Crop Prod*, 2012, **37**, 93-99.
19. E. Kalita, B. Nath, P. Deb, F. Agan, M. R. Islam and K. Saikia, *Carbohyd Polym*, 2015, **122**, 308-313.
20. P. Nascimento, R. Marim, G. Carvalho and S. Mali, *Mater Res Ibero Am J Mater*, 2016, **19**, 167-174.
21. W. Chen, Q. Li, Y. Wang, X. Yi, J. Zeng, H. Yu, Y. Liu and J. Li, *ChemSusChem*, 2014, **7**, 154-161.
22. N. Mohammed, A. Baidya, V. Murugesan, A. A. Kumar, M. A. Ganayee, J. S. Mohanty, K. C. Tam and T. Pradeep, *Acs Sustain Chem Eng*, 2016, **4**, 6167-6176.
23. P. R. Sharma, A. Chattopadhyay, S. K. Sharma, L. H. Geng, N. Amiralian, D. Martin and B. S. Hsiao, *Acs Sustain Chem Eng*, 2018, **6**, 3279-3290.
24. G. Metreveli, L. Wågberg, E. Emmoth, S. Belák, M. Strømme and A. Mihranyan, *Adv Healthc Mater*, 2014, **3**, 1546-1550.
25. A. Mautner, K.-Y. Lee, P. Lahtinen, M. Hakalahti, T. Tammelin, K. Li and A. Bismarck, *Chem Commun*, 2014, **50**, 5778-5781.
26. H. Ma, C. Burger, B. S. Hsiao and B. Chu, *Biomacromolecules*, 2011, **12**, 970-976.
27. T. Suopajärvi, H. Liimatainen, O. Hormi and J. Niinimäki, *Chem Eng J*, 2013, **231**, 59-67.
28. X. Sun, C. Danumah, Y. Liu and Y. Boluk, *Chem Eng J*, 2012, **198**, 476-481.
29. S. Ge, P. Champagne, H. Wang, P. G. Jessop and M. F. Cunningham, *Environ Sci Technol*, 2016, **50**, 7896-7903.

30. X. D. Wu, C. H. Lu, W. Zhang, G. P. Yuan, R. Xiong and X. X. Zhang, *J Mater Chem A*, 2013, **1**, 8645-8652.
31. N. Bossa, A. W. Carpenter, N. Kumar, C.-F. de Lannoy and M. Wiesner, *Environ Sci-Nano*, 2017, **4**, 1294-1303.
32. Z. Shi, J. Tang, L. Chen, C. Yan, S. Tanvir, W. A. Anderson, R. M. Berry and K. C. Tam, *J Mater Chem B*, 2015, **3**, 603-611.
33. A. L. Wani, A. Ara and J. A. Usmani, *Interdiscip Toxicol*, 2015, **8**, 55-64.
34. S. Dhanakumar, G. Solaraj and R. Mohanraj, *Ecotox Environ Safe*, 2015, **113**, 145-151.
35. H. Herrmann, J. Nolde, S. Berger and S. Heise, *Ecotox Environ Safe*, 2016, **124**, 213-238.
36. S. Kulaksız and M. Bau, *Environ Int*, 2011, **37**, 973-979.
37. T. Kameda, K. Hoshi and T. Yoshioka, *Solid State Sci*, 2011, **13**, 366-371.
38. M. Wang, X. Li, W. Hua, L. Shen, X. Yu and X. Wang, *ACS Appl Mater Interf*, 2016, **8**, 23995-24007.
39. Q. Zhou, H. Yang, C. Yan, W. Luo, X. Li and J. Zhao, *Colloids Surf A*, 2016, **501**, 9-16.
40. F. Zhao, E. Repo, Y. Song, D. Yin, S. B. Hammouda, L. Chen, S. Kalliola, J. Tang, K. C. Tam and M. Sillanpää, *Green Chem*, 2017, **19**, 4816-4828.
41. D. Wu, Y. Sun and Q. Wang, *J Hazard Mater*, 2013, **260**, 409-419.
42. Z. Birungi and E. Chirwa, *Bioresour Technol*, 2014, **160**, 43-51.
43. D. Das, C. J. S. Varshini and N. Das, *Miner Eng*, 2014, **69**, 40-56.
44. M. Torab-Mostaedi, M. Asadollahzadeh, A. Hemmati and A. Khosravi, *Res Chem Intermed*, 2015, **41**, 559-573.
45. T. Saito, T. Uematsu, S. Kimura, T. Enomae and A. Isogai, *Soft Matter*, 2011, **7**, 8804-8809.
46. T. Saito, S. Kimura, Y. Nishiyama and A. Isogai, *Biomacromolecules*, 2007, **8**, 2485-2491.
47. W. Wu, Q. He and C. Jiang, *Nanoscale Res Lett*, 2008, **3**, 397.
48. P. R. Sharma, R. Joshi, S. K. Sharma and B. S. Hsiao, *Biomacromolecules*, 2017, **18**, 2333-2342.
49. P. R. Sharma and A. J. Varma, *Chem Commun*, 2013, **49**, 8818-8820.
50. J. Navratil, *J Radioanal Nucl Chem*, 2001, **248**, 571-574.
51. A. K. Jha, A. Bose and J. P. Downey, *Sep Sci Technol*, 2006, **41**, 3297-3312.
52. Z. Surowiec, M. Budzyński, K. Durak and G. Czernel, *Nukleonika*, 2017, **62**, 73-77.
53. D. Predoi, *Dig J Nanomater Biostructures*, 2007, **2**, 169-173.
54. P. R. Sharma, B. Zheng, S. K. Sharma, C. Zhan, R. Wang, S. R. Bhatia and B. S. Hsiao, *ACS Appl Nano Mater*, 2018, **1**, 3969-3980.
55. P. R. Sharma, A. Chattopadhyay, C. Zhan, S. K. Sharma, L. Geng and B. S. Hsiao, *Cellulose*, 2018, **25**, 1961-1973.
56. P. Proll and L. Sutcliffe, *Trans Faraday Soc*, 1961, **57**, 1078-1087.
57. C. Zhan, Y. Li, P. R. Sharma, H. He, S. K. Sharma, R. Wang and B. S. Hsiao, *Rsc Adv*, 2019, **9**, 40565-40576.
58. Y. Li, J. Zhang, C. Zhan, F. Kong, W. Li, C. Yang and B. S. Hsiao, *Carbohyd Polym*, 2020, 115838.
59. E. M. Iannicelli-Zubiani, P. G. Stampino, C. Cristiani and G. Dotelli, *Chem Eng J*, 2018, **341**, 75-82.
60. E. M. Iannicelli-Zubiani, C. Cristiani, G. Dotelli and P. G. Stampino, *Waste Manag*, 2017, **60**, 582-590.

61. A. K. Mosai, L. Chimuka, E. M. Cukrowska, I. A. Kotzé and H. Tutu, *Water Air Soil Poll*, 2019, **230**, 188.
62. G. Li, C. J. Li, C. Zhang, Z. Y. Cheng, Z. Quan, C. Peng and J. Lin, *J Mater Chem*, 2009, **19**, 8936-8943.
63. Z. Shojaei, E. Iravani, M. Moosavian and M. Torab-Mostaedi, *Desalin Water Treat*, 2016, **57**, 27754-27767.
64. D. Wu, L. Zhang, L. Wang, B. Zhu and L. Fan, *J Chem Technol Biotechnol*, 2011, **86**, 345-352.
65. G. Hong, L. Shen, M. Wang, Y. Yang, X. Wang, M. Zhu and B. S. Hsiao, *Chem Eng J*, 2014, **244**, 307-316.
66. E. Kusrini, W. Wicaksono, C. Gunawan, N. Z. A. Daud and A. Usman, *J Environ Chem Eng*, 2018, **6**, 6580-6588.

TOC Graphic

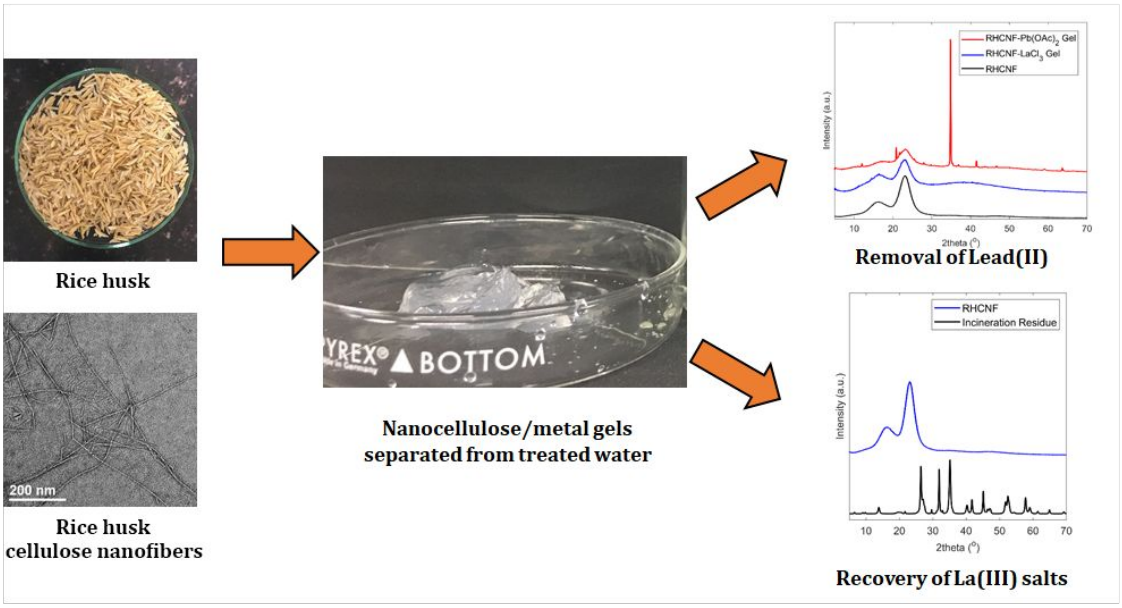

Nanocellulose scaffold derived from rice husk could efficiently remove heavy metal ions from contaminated water.